Brownian diffusion and thermophoresis mechanisms in Casson fluid over a moving wedge

Imran Ullah [a,b], Sharidan Shafie [a,*], Ilyas Khan [c], Kai Long Hsiao [d]

[a] Department of Mathematical Sciences, Faculty of Science, Universiti Teknologi Malaysia (UTM), 81310 Johor Bahru, Johor, Malaysia
[b] Department of Basic Sciences, National University of Sciences and Technology, Islamabad 44400, Pakistan
[c] Department of Basic Sciences, College of Engineering Majmaah University, Majmaah 11952, Saudi Arabia
[d] Department of Digital Recreation and Game Design, Taiwan Shoufu University, 168, Nansh Li District, Madou Jen, Tainan, Taiwan, ROC

ARTICLE INFO

ABSTRACT

The effect of Brownian diffusion and thermophoresis on electrically conducting mixed convection flow of Casson fluid induced by moving wedge is investigated in this paper. It is assumed that the wedge is saturated in a porous medium and experiences the thermal radiation and chemical reaction effects. The transformed nonlinear governing equations are solved numerically by Keller box scheme. Findings reveal that increase in Casson and magnetic parameters reduced the boundary layer thickness. The effect of Brownian motion and thermophoresis parameters are more pronounced on temperature profile as compared to nanoparticles concentration. The presence of thermal radiation assisted the heat transfer rate significantly. The influence of magnetic parameter is observed less significant on temperature and nanoparticles concentration.

Introduction

Nanofluids are engineered by dispersing a small quantity of nano-sized particles commonly less than 100 nm, which are uniformly and stably suspended into traditional fluids such as ethylene glycol, oil, water, lubricants, Bio-fluids and polymer solutions. During the last decades, researchers are prompted to discover alternate sources for energy due to fossil fuels deficiency. It is already proven that the addition of nanoparticles in working fluid can improve the performance of solar systems significantly, and can make them more efficient. Nanofluids also play a vital role in cooling and heating processes. Recently, the flow of nanofluids is of great interest in various areas of science, engineering and technology, chemical and nuclear industries and bio-mechanics. The term "nanofluid" was first coined by Choi and Eastman [1], and come up with a significant result that the thermal conductivity of base fluid can be enhanced by adding small amount of nano-sized particles. Later, Buongiorno [2] explore the convective transport in nanofluids. He observed that the absolute velocity of nanofluids can be expressed as the sum of base fluid velocity and relative slip velocity. In his significant research, he noticed that Brownian motion and thermophoresis dominate the other slip mechanism. The Cheng-Minkowycz problem for free convection flow of nanofluid over a vertical plate was studied by Nield and Kuznetsov [3]. Yacob et al. [4] studied steady boundary layer flow caused by static as well as moving wedge saturated in a nanofluid. They have considered water as base fluid for several nanoparticles. They obtained numerical solutions by Keller box method along with DO2HAF routine using similarity transformations. They noticed that velocity and temperature gradients grow as nanoparticles volume fraction and wedge angle parameter increased.

Khan et al. [5] discussed the similarity solutions of boundary layer flow of nanofluid over a wedge with convective boundary conditions. They assumed that the wedge is placed stationary in a nanofluid. Further, they considered water and ethylene glycol as base fluid for nanoparticles. They also observed that increase of convective parameter leads to enhance the velocity and temperature gradients. The influence of thermal radiation on two dimensional boundary layer flow of nanofluid over a vertical cone was investigated by Chamkha et al. [6]. RamReddy et al. [7] studied the Soret effect on nanofluid in the presence of convective boundary condition. Kasmani et al. [8] analyzed the influence of chemical reaction on two dimensional flow of nanofluid past a static wedge. They obtained the numerical solutions by fourth-order Runge-Kutta method along with shooting technique. They pointed out that the presence of chemical reaction weakens the nanoparticles concentration.

* Corresponding author.
E-mail address: sharidan@utm.com (S. Shafie).

In the recent years, the study of magnetohydrodynamic (MHD) has gained considerable attention due to its practical applications in numerous technologies, including, MHD power generators, cooling of nuclear reactors, construction of heat exchangers, installation of nuclear accelerators, blood flow measurement techniques and on the performance of several other systems employing electrically conducting fluids. On the other hand, magnetic nanofluids possess both the magnetic and liquid properties. External magnetic fields are useful to determine the thermal and physical nature of the nanofluids [9]. The effect of magnetic field on convective flow of viscous fluid past a wedge and cone embedded in porous medium was discussed by Chamkha [10]. Takhar et al. [11] investigated the effect of magnetic field on unsteady flow past a flat plate. The non-similar solutions for MHD flow of rotating fluid due to moving plate with Hall currents were presented by Takhar et al. [12]. On the other hand, Mudhaf and Chamkha [13] found the similarity solutions of hydromagnetic thermosolutal Marangoni convection flow of viscous fluid in the presence of heat generation and absorption. Chamkha et al. [14] discussed the influence of magnetic field on viscous fluid over a wedge in the presence of thermal radiation and heat source. They noticed higher temperature with increase in radiation parameter. Nandy and Mahapatra [15] analyzed the slip effects on stagnation point flow of nanofluid generated by stretching surface in the presence of heat generation and magnetic field. Rashidi et al. [16] examined the buoyancy effects on hydromagnetic flow of nanofluid due to stretching surface with thermal radiation. The two dimensional MHD forced and natural convection flow over non-isothermal wedge and cone saturated in a nanofluid was presented by Chamkha and Rashad [17]. They employed Buongiorno's model and analyzed the effects of Brownian motion and thermophoresis on flow fields. They noticed that increase of pressure gradient parameter enhances the fluid velocity, whereas reduction in temperature and nanoparticles concentration was observed. The two dimensional natural convection flow of nanofluid past a vertical cone through porous medium was reported by Chamkha and Rashad [18].

Chamkha [19] studied the effect of thermal radiation on natural convection about a truncated cone under the influence of magnetic field. Takhar et al. [20] and Chamkha and Mudhaf [21] analyzed mixed convection flow past a vertical cone in the absence and presence of heat generation and absorption. Chamkha et al. [22] investigated the effects of thermal radiation on mixed convection flow of nanofluid past a wedge saturated in a porous medium. They obtained numerical computations by Keller box method using non-similar transformations. They noticed that heat and mass transfer rates are increasing functions of thermal radiation parameter. They also predicted that thermophoresis parameter has similar effects on both temperature and nanoparticles concentration distributions.

Khan et al. [23] investigated thermal radiation effects on MHD mixed convection flow of viscous nanofluid caused by moving wedge under the influence of magnetic field and first order chemical reaction. They assumed that the wedge is stretching and contracting inside the nanofluid. They noted a significant change in temperature distribution as thermal convective parameter increased. They also noticed that thermal radiation parameter strengthen the temperature in the nanofluid. The variation of heat generation or absorption on mixed convection slip flow of nanofluid past a wedge was reported by Pandey and Kumar [24]. They assumed that the flow is electrically conducting and the medium is porous. They used Runge-Kutta-Fehlberg scheme via shooting procedure for numerical computations. Also, the effect of slip parameter on velocity and temperature profile was noticed opposite.

Due to the rapid growth of its applications, non-Newtonian fluids have attracted the attention of researchers in the last few decades. Several models have been reported in the existing literature. Among non-Newtonian fluid models is Casson model which is described as shear thinning liquid. The unique rheological characteristics have increased the importance of Casson fluid among other non-Newtonian fluids. These characteristics present shear stress-strain relationships that is distinct from Newtonian fluids. Damseh et al. [25] and Chamkha et al. [26] investigated steady and unsteady natural convection flow of micropolar fluid in the presence of chemical reaction. Mukhopadhyay and Mandal [27] investigated the two dimensional boundary layer flow of Casson fluid over a symmetric wedge. The chemical reaction behavior in the hydromagnetic mixed convection flow of Casson nanofluid over a stretching surface is examined by Ibrahim et al. [28]. In another study, Raju and Sandeep [29] examined electrically conducting flow of Casson nanofluid generated due to moving wedge. They assumed the convecting heating at temperature wall. They transformed the governing equations using similarity transformations, and achieved numerical solutions via Runge-Kutta and Newton's methods. Further, they seen that the behavior of Brownian motion and thermophoresis parameter is opposite on temperature field.

The literature mentioned demonstrates that no attempt is made to study the mixed convection flow of Casson nanofluid over a moving wedge. The objective of present analysis is to investigate the influence of electrically conducting mixed convection flow of Casson nanofluid generated by a moving wedge in the presence of thermal radiation. The mathematical computations are carried out by applying Keller-box method [30]. Graphs are revealed and discussed for pertinent parameters. Comparisons of some exceptional cases are made with the existing results and achieved a good agreement.

Mathematical formulation

Two dimensional hydromagnetic mixed convection flow of Casson nanofluid generated due to moving wedge is considered. It is assumed that the wedge is moving through porous medium in the presence of chemical reaction and thermal radiation. The velocity of wedge and free stream velocity are $u_w(x) = U_w x^m$ and $u_e(x) = U_\infty x^m$, respectively, where U_w, U_∞ are constants and $m = \frac{\beta_1}{(2-\beta_1)}$, β_1 is the Hartree pressure gradient parameter that corresponds to $\beta_1 = \frac{\Omega}{\pi}$ for the total angle $\Omega = \beta_1 \pi$ of the wedge (see Fig. 1). A transverse magnetic field $B(x) = B_0 x^{(m-1)/2}$ [29] is applied in the y-direction with strength B_0. The temperature and nanoparticles concentration at wall and free stream are T_f, C_s, T_∞ and C_∞, respectively.
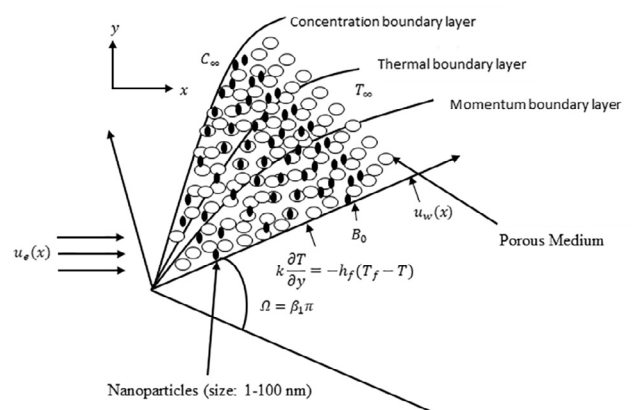

Fig. 1. Physical model and coordinate system.

The governing equations for Casson nanofluid along with continuity equation are given as

$$\frac{\partial u}{\partial x} + \frac{\partial v}{\partial y} = 0 \quad (1)$$

$$u\frac{\partial u}{\partial x} + v\frac{\partial u}{\partial y} = u_e\frac{\partial u_e}{\partial x} + v\left(1 + \frac{1}{\beta}\right)\frac{\partial^2 u}{\partial y^2} + \left(\frac{\sigma B^2(x)}{\rho} + \left(1 + \frac{1}{\beta}\right)\frac{v\varphi}{k_1}\right)(u_e - u)$$
$$+ \left[(1 - C_\infty)\rho_{f_\infty}\beta_T(T - T_\infty) - (\rho_p - \rho_{f_\infty})\beta_C(C - C_\infty)\right]g\sin\frac{\Omega}{2} \quad (2)$$

$$u\frac{\partial T}{\partial x} + v\frac{\partial T}{\partial y} = \alpha_f\frac{\partial^2 T}{\partial y^2} + \tau\left[D_B\frac{\partial C}{\partial y}\frac{\partial T}{\partial y} + \frac{D_T}{T_\infty}\left(\frac{\partial T}{\partial y}\right)^2\right] - \frac{1}{(\rho c)_f}\frac{\partial q_r}{\partial y}, \quad (3)$$

$$u\frac{\partial C}{\partial x} + v\frac{\partial C}{\partial y} = D_B\frac{\partial^2 C}{\partial y^2} + \frac{D_T}{T_\infty}\frac{\partial^2 T}{\partial y^2} - k_c(C - C_\infty) \quad (4)$$

where v is kinematic viscosity, σ is the electrically conductivity, β is the Casson parameter, ρ_f is the fluid density, ϕ is the porosity, $k_1(x) = k_0/x^{(m-1)}$ is the permeability of porous medium, g is the gravitational force due to acceleration, ρ_p is the density of nanoparticles, β_T is the volumetric coefficient of thermal expansion, β_C the coefficient of concentration expansion, $\alpha_f = \frac{k}{(\rho c)_f}$ is the thermal diffusivity of the Casson fluid, k is the thermal conductivity of fluid, $(\rho c)_f$ is the heat capacity of the fluid, $\tau = \frac{(\rho c)_p}{(\rho c)_f}$ is the ratio of heat capacities, $(\rho c)_p$ is the effective heat capacity of nanoparticles material, D_B is the Brownian diffusion coefficient, D_T is the thermophoretic diffusion coefficient, q_r is the radiative heat flux and $k_c(x) = ak_2 x^{m-1}$ is the variable rate of chemical reaction k_2 is a constant reaction rate and a is the reference length along the flow.

The corresponding boundary conditions are written as follows:

$$u = u_w(x) + N_1 v\left(1 + \frac{1}{\beta}\right)\frac{\partial u}{\partial y} \quad k\frac{\partial T}{\partial y} = -h_f(T_f - T),$$
$$D_B\frac{\partial C}{\partial y} = -h_s(C_s - C) \text{ at } y = 0, \quad (5)$$

$$u \to u_e(x), \quad T \to T_\infty, \quad C \to C_\infty \text{ as } y \to \infty \quad (6)$$

Here $N_1(x) = N_0 x^{-\frac{m-1}{2}}$ [31] is the velocity slip factor with constant N_0, $h_f(x) = h_0 x^{\frac{m-1}{2}}$ [5] and $h_s(x) = h_1 x^{\frac{m-1}{2}}$ are the convective heat and mass transfer, respectively, $T_f(x) = T_\infty + T_0 x^{2m-1}$ and $C_s(x) = C_\infty + C_0 x^{2m-1}$.

The radiative heat flux q_r described according to Rosseland approximation is give as

$$q_r = \frac{-4\sigma^*}{3k_1^*}\frac{\partial T^4}{\partial y} \quad (7)$$

where σ^*, k_1^* are the Stefan-Boltzmann constant and mean absorption coefficient, respectively. By expanding T^4 in a Taylor series about T_∞ and neglecting higher terms, obtained

$$T^4 \cong 4T_\infty^3 T - 3T_\infty^4 \quad (8)$$

Using Eq. (7) and Eq. (8) in Eq. (3), expressed as

$$u\frac{\partial T}{\partial x} + v\frac{\partial T}{\partial y} = \alpha_f\frac{\partial^2 T}{\partial y^2} + \frac{16\sigma^* T_\infty^3}{3\rho c_p k_1^*}\frac{\partial^2 T}{\partial y^2}$$
$$+ \tau\left[D_B\frac{\partial C}{\partial y}\frac{\partial T}{\partial y} + \frac{D_T}{T_\infty}\left(\frac{\partial T}{\partial y}\right)^2\right] \quad (9)$$

Now use the following similarity transformations the following similarity transformations;

$$\psi = \sqrt{\frac{2vU_\infty}{(m+1)}}x^{\frac{m+1}{2}}f(\eta), \eta = \sqrt{\frac{(m+1)U_\infty}{2v}}x^{\frac{m-1}{2}}y,$$

$$\theta(\eta) = \frac{T - T_\infty}{T_f - T_\infty}, \phi(\eta) = \frac{C - C_\infty}{C_s - C_\infty} \quad (10)$$

where ψ is the stream function and satisfies Eq. (1).

The system of Eqs. (3)–(7) and Eq. (9) can be expressed as

$$\left(1 + \frac{1}{\beta}\right)f''' + ff'' + \frac{2m}{m+1}(1 - f'^2) + \frac{2}{(m+1)}\left(M + \left(1 + \frac{1}{\beta}\right)K\right)(1 - f')$$
$$+ \frac{2}{(m+1)}(Gr_n\theta - Gm_n\phi)\sin\left(\frac{2m}{m+1}\frac{\pi}{2}\right) = 0, \quad (11)$$

$$\frac{1}{Pr}\left(1 + \frac{4}{3}R_d\right)\theta'' + f\theta' - 2\left(\frac{2m-1}{m+1}\right)f'\theta + N_b\phi'\theta' + N_t\theta'^2 = 0, \quad (12)$$

$$\frac{1}{Le}\phi'' + f\phi' - 2\left(\frac{2m-1}{m+1}\right)f'\phi + \frac{N_t}{N_b}\theta'' - \frac{2}{(m+1)}R\phi = 0, \quad (13)$$

The associated boundary conditions are given as

$$\left.\begin{array}{l}f'(0) = \gamma + \delta\sqrt{\frac{m+1}{2}}\left(1 + \frac{1}{\beta}\right)f''(0), \quad \theta'(0) = -\left(\sqrt{\frac{2}{m+1}}\right)Bi_1[1 - \theta(0)] \\ \phi'(0) = -\left(\sqrt{\frac{2}{m+1}}\right)Bi_2[1 - \phi(0)]\end{array}\right\}, \quad (14)$$

$$f'(\infty) = 1, \theta(\infty) = 0, \phi(\infty) = 0 \quad (15)$$

In the above expressions, M, K, Gr_n, Gm_n, δ, Pr, R_d, N_b, N_t, Bi_1, Bi_2, Le and R ($R > 0$ corresponds to destructive chemical reaction and $R < 0$ represents generative chemical reaction), are the magnetic parameter, porosity parameter, thermal Grashof number, mass Grashof number, slip parameter, Prandtl number, radiation parameter, Brownian motion parameter, thermophoresis parameter, Biot numbers, Lewis number and chemical reaction parameter, and are defined as

$$M = \frac{\sigma B_0^2}{\rho U_\infty}, \quad K = \frac{v\varphi}{k_0 U_\infty}, \quad Gr_n = \frac{g\beta_T(1 - C_\infty)\rho_{f_\infty}T_0}{v^2\rho_f},$$

$$Gm_n = \frac{g\beta_C(\rho_p - \rho_{f_\infty})C_0}{v^2\rho_f}, \quad \delta = N_0\sqrt{U_\infty v}, \quad Pr = \frac{v}{\alpha_f},$$

$$R_d = \frac{4\sigma^* T_\infty^3}{kk_1^*}, \quad N_b = \frac{\tau D_B(C_s - C_\infty)}{v}, \quad N_t = \frac{\tau D_T(T_f - T_\infty)}{v},$$

$$Bi_1 = \frac{h_0}{k}\left[\frac{v}{U_\infty}\right]^{1/2} Bi_2 = \frac{h_1}{D_B}\left[\frac{v}{U_\infty}\right]^{1/2}, \quad Le = \frac{v}{D_B}, \quad R = \frac{vak_2}{U_\infty}$$

The wall skin friction, wall heat flux and wall mass flux, respectively, are defined by

$$\tau_w = \mu_B\left(1 + \frac{1}{\beta}\right)\left[\frac{\partial u}{\partial y}\right]_{y=0},$$

$$q_w = -\left(\left(\alpha + \frac{16\sigma^* T_\infty^3}{3\rho c_p k_1^*}\right)\frac{\partial T}{\partial y}\right)_{y=0} \text{ and } q_s = -D_B\left(\frac{\partial C}{\partial y}\right)_{y=0} \quad (16)$$

The quantities of physical interest are skin friction coefficient $Cf_x = \frac{\tau_w}{\rho u_w^2}$, Nusselt number $Nu_x = \frac{xq_w}{\alpha(T_f - T_\infty)}$ and Sherwood number $Sh_x = \frac{xq_s}{D_B(C_s - C_\infty)}$, and are defined by

$$(Re_x)^{1/2}Cf_x = \sqrt{\frac{m+1}{2}}\left(1 + \frac{1}{\beta}\right)f''(0),$$

$$(Re_x)^{-1/2}Nu_x = -\sqrt{\frac{m+1}{2}}\left(1 + \frac{4}{3}R_d\right)\theta'(0),$$

$$(Re)^{-1/2}Sh_x = -\left(\sqrt{\frac{m+1}{2}}\right)\phi'(0) \quad (17)$$

Numerical solutions

The numerical computations for the nonlinear ordinary differential Eqs. (11)–(13) subject to boundary conditions (14) and (15) are obtained through Keller-box method. It is a common belief that this method is unconditionally stable and is suitable for the parabolic equations. This method further comprises of three methods, and the details are given as

The finite difference method

Firstly, the governing equations need to be converted to first order differential equations. The new independent variables are introduced for $f(\eta)$, $u(\eta)$, $v(\eta)$, $g(\eta)$, $s(\eta)$, $p(\eta)$, $q(\eta)$. Also, $\theta(\eta)$ and $\varphi(\eta)$ are replaced by $g(\eta)$ and $p(\eta)$, respectively, that correspond to temperature and concentration respectively. Therefore, the first order equations are of the form

$$F'(\eta) = u(\eta), \tag{18}$$

$$U'(\eta) = v(\eta), \tag{19}$$

$$G'(\eta) = s(\eta), \tag{20}$$

$$P'(\eta) = q(\eta), \tag{21}$$

$$\left(1 + \frac{1}{\beta}\right)v' + fv - \left(\frac{2m}{m+1}\right)(1 - u^2) - \frac{2}{m+1}\left(M + \left(1 + \frac{1}{\beta}\right)K\right)(1 - u)$$
$$+ \frac{2}{m+1}(Gr_n g + Gm_n p) = 0, \tag{22}$$

$$\frac{1}{Pr}\left(1 + \frac{4}{3}R_d\right)s' + fs - 2\left(\frac{2m-1}{m+1}\right)ug + N_b qs + N_t s^2 = 0 \tag{23}$$

$$\frac{1}{Sc}q' + fq - 2\left(\frac{2m-1}{m+1}\right)up + \frac{N_t}{N_b}s' - \frac{2}{(m+1)}Rp = 0, \tag{24}$$

The associated boundary conditions in terms of η, becomes (Fig. 2.)

$$\left.\begin{array}{c} f(\eta) = 0, u(\eta) = \gamma + \delta\sqrt{\frac{m+1}{2}}\left(1 + \frac{1}{\beta}\right)v(\eta), \ s(\eta) = -\left(\sqrt{\frac{2}{m+1}}\right)Bi_1[1 - g(\eta)] \\ q(\eta) = -\left(\sqrt{\frac{2}{m+1}}\right)Bi_2[1 - p(\eta)] at \eta = 0 \end{array}\right\}, \tag{25}$$

$$u(\eta) \to 1, \quad g(\eta) \to 0, \quad p(\eta) \to 0 \quad as \quad \eta \to \infty. \tag{26}$$

The net rectangle is considered in the $x - \eta$ plane as shown in Figue 2, and the net points are defined as follow:

$$x^0 = 0, \quad x^i = x^{i-1} + k_i, \quad i = 1, 2, 3, \ldots I, \eta_0 = 0,$$
$$\eta_j = \eta_{j-1} + h_j, \quad j = 1, 2, 3, \ldots J,$$

where k_i is the Δx–spacing and h_j is the $\Delta \eta$–spacing. Here i and j are just sequence of numbers that indicate the coordinate location, not tensor indices or exponents.

The derivatives in the x–direction are given by finite difference, for example

$$\frac{\partial u}{\partial x} = \frac{u^i - u^{i-1}}{k_i},$$

while the derivatives in the η– direction are replaced by finite difference, for example

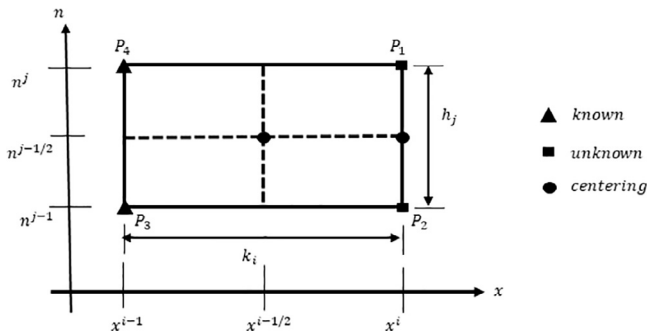$$V' = \frac{\partial v}{\partial \eta} = \frac{v_j - v_{j-1}}{h_j},$$

For any points:

Fig. 2. Net rectangle for difference approximations.

$$()_j^{i-1/2} = \frac{1}{2}\left[()_j^i + ()_j^{i-1}\right], \quad ()_{j-1/2}^i = \frac{1}{2}\left[()_j^i + ()_{j-1}^i\right],$$

Using centered–difference derivatives, the finite difference approximations of the ordinary differential Eqs. (18)–(24) are written for the midpoint $(\eta_{j-1/2})$ of the segment $P_1 P_2$. The process is called "centering about $(x^i, \eta_{j-1/2})$"

$$\frac{\left(f_j^i - f_{j-1}^i\right)}{h_j} = \frac{1}{2}\left(u_j^i + u_{j-1}^i\right) = u_{j-1/2}^i, \tag{27}$$

$$\frac{\left(u_j^i - u_{j-1}^i\right)}{h_j} = \frac{1}{2}\left(v_j^i + v_{j-1}^i\right) = v_{j-1/2}^i, \tag{28}$$

$$\frac{\left(s_j^i - s_{j-1}^i\right)}{h_j} = \frac{1}{2}\left(g_j^i + g_{j-1}^i\right) = g_{j-1/2}^i, \tag{29}$$

$$\frac{\left(q_j^i - q_{j-1}^i\right)}{h_j} = \frac{1}{2}\left(p_j^i + p_{j-1}^i\right) = p_{j-1/2}^i, \tag{30}$$

$$\left(1 + \frac{1}{\beta}\right)\frac{(v_j^i - v_{j-1}^i)}{h_j} + \left[\left(\frac{f_j^i + f_{j-1}^i}{2}\right)\left(\frac{v_j^i + v_{j-1}^i}{2}\right)\right]$$
$$- \left(\frac{2m}{m+1}\right)\left[1 - \left(\frac{u_j^i + u_{j-1}^i}{2}\right)^2\right]$$
$$- \frac{2}{m+1}\left(M + \left(1 + \frac{1}{\beta}\right)K\right)\left[1 - \left(\frac{u_j^i + u_{j-1}^i}{2}\right)\right]$$
$$+ \frac{2}{m+1}Gr_n\left(\frac{g_j^i + g_{j-1}^i}{2}\right)\sin\left(\frac{2m}{m+1}\frac{\pi}{2}\right)$$
$$+ \frac{2m}{m+1}Gm_n\left(\frac{p_j^i + p_{j-1}^i}{2}\right)\sin\left(\frac{2m}{m+1}\frac{\pi}{2}\right) = L_{j-1/2} \tag{31}$$

$$\frac{1}{Pr}\left(1 + \frac{4}{3}R_d\right)\left(\frac{s_j^i - s_{j-1}^i}{h_j}\right) + \left[\left(\frac{f_j^i + f_{j-1}^i}{2}\right)\left(\frac{s_j^i + s_{j-1}^i}{2}\right)\right]$$
$$- \left(\frac{2m-1}{m+1}\right)\left[\left(\frac{u_j^i + u_{j-1}^i}{2}\right)\left(\frac{g_j^i + g_{j-1}^i}{2}\right)\right]$$
$$+ N_b\left(\frac{q_j^i + q_{j-1}^i}{2}\right)\left(\frac{s_j^i + s_{j-1}^i}{2}\right) + N_t\left(\frac{s_j^i + s_{j-1}^i}{2}\right)^2 = N_{j-1/2}, \tag{32}$$

$$\frac{1}{Sc}\left(\frac{q_j^i - q_{j-1}^i}{h_j}\right) + \left(\frac{f_j^i + f_{j-1}^i}{2}\right)\left(\frac{q_j^i + q_{j-1}^i}{2}\right) - 2\left(\frac{2m-1}{m+1}\right)\left(\frac{u_j^i + u_{j-1}^i}{2}\right)$$
$$\times \left(\frac{p_j^i + p_{j-1}^i}{2}\right) + \frac{N_b}{N_t}\left(\frac{s_j^i - s_{j-1}^i}{h_j}\right) - \frac{2}{(m+1)}R\left(\frac{p_j^i + p_{j-1}^i}{2}\right) = Q_{j-1/2} \tag{33}$$

where

$$
L_{j-1/2} = - \begin{bmatrix} \left(1 + \frac{1}{\beta}\right)\frac{\left(v_j^{i-1} - v_{j-1}^{i-1}\right)}{h_j} + \left[\left(\frac{f_j^{i-1} + f_{j-1}^{i-1}}{2}\right)\left(\frac{v_j^{i-1} + v_{j-1}^{i-1}}{2}\right)\right] - \left(\frac{2m}{m+1}\right)\left[1 - \left(\frac{u_j^{i-1} + u_{j-1}^{i-1}}{2}\right)^2\right] \\ -\frac{2}{m+1}\left(M + (1+\frac{1}{\beta})K\right)\left[1 - \left(\frac{u_j^{i-1} + u_{j-1}^{i-1}}{2}\right)\right] + \frac{2}{m+1}Gr_n\left(\frac{g_j^{i-1} + g_{j-1}^{i-1}}{2}\right)\sin\left(\frac{2m}{m+1}\frac{\pi}{2}\right) \\ +\frac{2}{m+1}Gm_n\left(\frac{p_j^{i-1} + p_{j-1}^{i-1}}{2}\right)\sin\left(\frac{2m}{m+1}\frac{\pi}{2}\right) \end{bmatrix}
$$

$$
N_{j-1/2} = - \begin{bmatrix} \frac{1}{\Pr}\left(1 + \frac{4}{3}R_d\right)\left(\frac{s_j^{i-1} - s_{j-1}^{i-1}}{h_j}\right) + \left[\left(\frac{f_j^{i-1} + f_{j-1}^{i-1}}{2}\right)\left(\frac{s_j^{i-1} + s_{j-1}^{i-1}}{2}\right)\right] \\ -2\left(\frac{2m-1}{m+1}\right)\left[\left(\frac{u_j^{i-1} + u_{j-1}^{i-1}}{2}\right)\left(\frac{g_j^{i-1} + g_{j-1}^{i-1}}{2}\right)\right] \\ +N_b\left(\frac{q_j^{i-1} + q_{j-1}^{i-1}}{2}\right)\left(\frac{s_j^{i-1} + s_{j-1}^{i-1}}{2}\right) + N_t\left(\frac{s_j^{i-1} + s_{j-1}^{i-1}}{2}\right)^2 \end{bmatrix}
$$

$$
Q_{j-1/2} = - \begin{bmatrix} \frac{1}{Sc}\left(\frac{q_j^{i-1} - q_{j-1}^{i-1}}{h_j}\right) + \left(\frac{f_j^{i-1} + f_{j-1}^{i-1}}{2}\right)\left(\frac{q_j^{i-1} + q_{j-1}^{i-1}}{2}\right) - 2\left(\frac{2m-1}{m+1}\right)\left(\frac{u_j^{i-1} + u_{j-1}^{i-1}}{2}\right)\left(\frac{p_j^{i-1} + p_{j-1}^{i-1}}{2}\right) \\ +\frac{N_b}{N_t}\left(\frac{s_j^{i-1} - s_{j-1}^{i-1}}{h_j}\right) - \frac{2}{(m+1)}R\left(\frac{p_j^{i-1} + p_{j-1}^{i-1}}{2}\right) \end{bmatrix}
$$

At $x = x^i$, the subjected boundary conditions (25) and (26) in terms of the dependent variable η become

$$
\left.\begin{array}{l} f_o^i = 0, u_o^i = 1 + \delta\left(1 + \frac{1}{\beta}\right)v_o^i, s_o^i = -\left(\sqrt{\frac{2}{n+1}}\right)Bi_1[1 - g_o^i], \\ q_o^i = -\left(\sqrt{\frac{2}{n+1}}\right)Bi_2[1 - p_o^i] \end{array}\right\} \tag{34}
$$

$$
u_J^i = 1, g_J^i = 0, p_J^i = 0, \tag{35}
$$

Newton's method

Newton's method is used to linearize the nonlinear system of equations. For this purpose, following iterates are introduced

$$
\begin{aligned} &f_j^{(k+1)} = f_j^k + \delta f_j^k, u_j^{(k+1)} = u_j^k + \delta u_j^k, v_j^{(k+1)} = v_j^k + vf_j^k, \\ &g_j^{(k+1)} = g_j^k + \delta g_j^k, s_j^{(k+1)} = s_j^k + \delta s_j^k, p_j^{(k+1)} = p_j^k + \delta p_j^k, \\ &q_j^{(k+1)} = q_j^k + \delta q_j^k. \end{aligned} \tag{36}
$$

Now using Eq. (36) into Eqs. (27)–(33), and after dropping the quadratic and higher order terms in $\delta f_j^{(k)}$, $\delta u_j^{(k)}$, $\delta v_j^{(k)}$, $\delta g_j^{(k)}$, $\delta s_j^{(k)}$, $\delta p_j^{(k)}$ and $\delta q_j^{(k)}$ as well as the superscript i for simplicity, this procedure yields the following linear tridiagonal system

$$
\delta f_j - \delta f_{j-1} - \frac{h_j}{2}(\delta u_j - \delta u_{j-1}) = (r_1)_{j-1/2}, \tag{37}
$$

$$
\delta u_j - \delta u_{j-1} - \frac{h_j}{2}(\delta v_j - \delta v_{j-1}) = (r_2)_{j-1/2}, \tag{38}
$$

$$
\delta g_j - \delta g_{j-1} - \frac{h_j}{2}(\delta s_j - \delta s_{j-1}) = (r_3)_{j-1/2}, \tag{39}
$$

$$
\delta p_j - \delta p_{j-1} - \frac{h_j}{2}(\delta q_j - \delta q_{j-1}) = (r_4)_{j-1/2}, \tag{40}
$$

$$
\begin{aligned} &(a_1)_j\delta v_j + (a_2)_j\delta v_{j-1} + (a_3)_j\delta f_j + (a_4)_j\delta f_{j-1} + (a_5)_j\delta u_j \\ &\quad + (a_6)_j\delta u_{j-1} + (a_7)_j\delta g_j + (a_8)_j\delta g_{j-1} + (a_9)_j\delta p_j + (a_{10})_j\delta p_{j-1} \\ &\quad = (r_5)_{j-1/2}, \end{aligned} \tag{41}
$$

$$
\begin{aligned} &(b_1)_j\delta s_j + (b_2)_j\delta s_{j-1} + (b_3)_j\delta f_j + (b_4)_j\delta f_{j-1} + (b_5)_j\delta u_j \\ &\quad + (b_6)_j\delta u_{j-1} + (b_7)_j\delta g_j + (b_8)_j\delta g_{j-1} + (b_9)_j\delta q_j + (b_{10})_j\delta q_{j-1} \\ &\quad = (r_6)_{j-1/2}, \end{aligned} \tag{42}
$$

$$
\begin{aligned} &(d_1)_j\delta q_j + (d_2)_j\delta q_{j-1} + (d_3)_j\delta f_j + (d_4)_j\delta f_{j-1} + (d_5)_j\delta u_j \\ &\quad + (d_6)_j\delta u_{j-1} + (d_7)_j\delta p_j + (d_8)_j\delta p_{j-1} + (d_9)_j\delta s_j + (d_{10})_j\delta s_{j-1} \\ &\quad = (r_7)_{j-1/2}, \end{aligned} \tag{43}
$$

where

$$
(a_1)_j = \left(1 + \frac{1}{\beta}\right) + \frac{h_j}{2}f_{j-1/2}, \tag{44}
$$

$$
(a_2)_j = -\left(1 + \frac{1}{\beta}\right) + \frac{h_j}{2}f_{j-1/2}, \tag{45}
$$

$$
(a_3)_j = \frac{h_j}{2}v_{j-1/2}, \tag{46}
$$

$$
(a_4)_j = (a_3)_j, \tag{47}
$$

$$
(a_5)_j = -\left(\frac{2m}{m+1}\right)h_j u_{j-1/2} - \left(\frac{2}{m+1}\right)\frac{h_j}{2}\left(M + \left(1 + \frac{1}{\beta}\right)K\right), \tag{48}
$$

$$
(a_6)_j = (a_5)_j, \tag{49}
$$

$$
(a_7)_j = \left(\frac{2}{m+1}\right)\frac{h_j}{2}Gr_n, \tag{50}
$$

$$
(a_8)_j = (a_7)_j, \tag{51}
$$

$$
(a_9)_j = \left(\frac{2}{m+1}\right)\frac{h_j}{2}Gm_n, \tag{52}
$$

$$
(a_{10})_j = (a_9)_j, \tag{53}
$$

$$
(b_1)_j = \frac{1}{\Pr}\left(1 + \frac{4}{3}R_d\right) + \frac{h_j}{2}f_{j-1/2}, \tag{54}
$$

$$
(b_2)_j = -\frac{1}{\Pr}\left(1 + \frac{4}{3}R_d\right) + \frac{h_j}{2}f_{j-1/2}, \tag{55}
$$

$$
(b_3)_j = \frac{h_j}{2}s_{j-1/2}, \tag{56}
$$

$$
(b_5)_j = -2\left(\frac{2m-1}{m+1}\right)\frac{h_j}{2}g_{j-1/2}, \tag{57}
$$

$$
(b_6)_j = (b_5)_j, \tag{58}
$$

$$
(b_7)_j = -2\left(\frac{2m-1}{m+1}\right)\frac{h_j}{2}u_{j-1/2}, \tag{59}
$$

$$
(b_8)_j = (b_7)_j, \tag{60}
$$

$$
(b_9)_j = \frac{h_j}{2}N_b s_{j-1/2}, \tag{61}
$$

$$
(b_{10})_j = (b_9)_j, \tag{62}
$$

$$
(d_1)_j = \frac{1}{Le} + \frac{h_j}{2}f_{j-1/2}, \tag{63}
$$

$$
(d_2)_j = -\frac{1}{Le} + \frac{h_j}{2}f_{j-1/2}, \tag{64}
$$

$$
(d_3)_j = \frac{h_j}{2}q_{j-1/2}, \tag{65}
$$

$$(d_4)_j = (d_3)_j, \tag{66}$$

$$(d_5)_j = -2\left(\frac{2m-1}{m+1}\right)\frac{h_j}{2}p_{j-1/2}, \tag{67}$$

$$(d_6)_j = (d_5)_j, \tag{68}$$

$$(d_7)_j = \frac{N_t}{N_b}, \tag{69}$$

$$(d_8)_j = -(d_7)_j, \tag{70}$$

and

$$(r_1)_{j-1/2} = f_j - f_{j-1} + h_j u_{j-1/2}, \tag{71}$$

$$(r_2)_{j-1/2} = u_j - u_{j-1} + h_j v_{j-1/2}, \tag{72}$$

$$(r_3)_{j-1/2} = g_j - g_{j-1} + h_j s_{j-1/2}, \tag{73}$$

$$(r_4)_{j-1/2} = p_j - p_{j-1} + h_j q_{j-1/2},$$

$$
\begin{aligned}
(r_5)_{j-1/2} = &\left(1+\frac{1}{\beta}\right)(v_{j-1} - v_j) - h_j f_{j-1/2} v_{j-1/2} \\
&+ \frac{2m}{m+1}h_j u_{j-1/2}^2 + \frac{2m}{m+1}h_j M u_{j-1/2} \\
&+ \frac{2m}{m+1}h_j\left(1+\frac{1}{\beta}\right)u_{j-1/2} \\
&- \frac{2}{m+1}h_j\left(Grg_{j-1/2} + Gmp_{j-1/2}\right)\sin\left(\frac{2}{m+1}\frac{\pi}{2}\right) \\
&+ L_{j-1/2},
\end{aligned}
\tag{74}
$$

$$
\begin{aligned}
(r_6)_{j-1/2} = &\frac{1}{\Pr}\left(1+\frac{4}{3}R_d\right)(s_{j-1} - s_j) - h_j f_{j-1/2} s_{j-1/2} \\
&+ \frac{2(2m-1)}{m+1}h_j u_{j-1/2} g_{j-1/2} + N_b h_j s_{j-1/2} q_{j-1/2} \\
&+ N_t h_j s_{j-1/2}^2 + N_{j-1/2},
\end{aligned}
\tag{75}
$$

$$
\begin{aligned}
(r_7)_{j-1/2} = &\frac{1}{Le}(q_{j-1} - q_j) - h_j f_{j-1/2} q_{j-1/2} \\
&+ \frac{2(2m-1)}{m+1}h_j u_{j-1/2} p_{j-1/2} + (s_{j-1} - s_j)\frac{N_t}{N_b} \\
&+ \frac{2}{n+1}h_j R p_{j-1/2} + Q_{j-1/2},
\end{aligned}
\tag{76}
$$

To complete the system, the boundary conditions (34) and (35) are recalled that can be satisfied exactly with no iteration (Cebeci and Bradshaw, 1988). So, the correct values in all the iterations are maintained by taking

$$\delta f_0 = 0, \quad \delta u_0 = 0, \quad \delta g_0 = 0, \quad \delta p_0 = 0, \quad \delta u_J = 0, \quad \delta g_J$$
$$= 0, \quad \delta p_J = 0 \tag{77}$$

The block-elimination method

The linearized differential equations of the system (37)–(43) have a block-tridiagonal structure. In vector-matrix form, it can be written as

$$[A][\delta] = [r], \tag{78}$$

where

$$
[A] = \begin{bmatrix}
[A_1] & [C_1] & 0 & 0 & 0 & 0 & 0 \\
[B_2] & [A_2] & [C_2] & 0 & 0 & 0 & 0 \\
0 & 0 & 0 & \ddots & 0 & 0 & 0 \\
0 & 0 & 0 & \ddots & 0 & 0 & 0 \\
0 & 0 & 0 & \ddots & 0 & 0 & 0 \\
0 & 0 & 0 & 0 & [B_{J-1}] & [A_{J-1}] & [C_{J-1}] \\
0 & 0 & 0 & 0 & 0 & [B_J] & [C_J]
\end{bmatrix}, [\delta] = \begin{bmatrix}
[\delta_1] \\
[\delta_2] \\
\vdots \\
[\delta_{J-1}] \\
[\delta_J]
\end{bmatrix},
$$

$$
[r] = \begin{bmatrix}
[r_1] \\
[r_2] \\
\vdots \\
[r_{J-1}] \\
[r_J]
\end{bmatrix},
$$

The block-tridiagonal structure are commonly consisting of variables or constants, but interestingly it consists of block matrices. By taking $e_j = -\frac{h_j}{2}$, the elements of matrices are defined as follows

$$
[A_1] = \begin{bmatrix}
0 & 0 & 0 & 1 & 0 & 0 & 0 \\
e_1 & 0 & 0 & 0 & e_1 & 0 & 0 \\
0 & e_1 & 0 & 0 & 0 & e_1 & 0 \\
0 & 0 & e_1 & 0 & 0 & 0 & e_1 \\
(a_2)_1 & 0 & 0 & (a_3)_1 & (a_1)_1 & 0 & 0 \\
0 & (b_2)_1 & (b_{10})_1 & (b_3)_1 & (b_1)_1 & (b_9)_1 & 0 \\
0 & (d_{10})_1 & (d_2)_1 & (d_3)_1 & 0 & (d_9)_1 & (d_1)_1
\end{bmatrix},
\tag{79}
$$

$$
[A_j] = \begin{bmatrix}
e_j & 0 & 0 & 1 & 0 & 0 & 0 \\
-1 & 0 & 0 & 0 & e_j & 0 & 0 \\
0 & -1 & 0 & 0 & 0 & e_j & 0 \\
0 & 0 & -1 & 0 & 0 & 0 & e_j \\
(a_6)_j & (a_8)_j & (a_{10})_j & (a_3)_j & (a_1)_j & 0 & 0 \\
(b_6)_j & (b_8)_j & 0 & (b_3)_j & 0 & (b_1)_j & (b_9)_j \\
(d_6)_j & 0 & (d_8)_j & (d_3)_j & 0 & (d_9)_j & (d_1)_j
\end{bmatrix}, 2 \leqslant j \leqslant J
\tag{80}
$$

$$
[B_j] = \begin{bmatrix}
0 & 0 & 0 & -1 & 0 & 0 & 0 \\
0 & 0 & 0 & 0 & e_j & 0 & 0 \\
0 & 0 & 0 & 0 & 0 & e_j & 0 \\
0 & 0 & 0 & 0 & 0 & 0 & e_j \\
0 & 0 & 0 & (a_4)_j & (a_2)_j & 0 & 0 \\
0 & 0 & 0 & (b_4)_j & 0 & (b_2)_j & (b_{10})_j \\
0 & 0 & 0 & (d_4)_j & 0 & 0 & (d_2)_j
\end{bmatrix} 2 \leqslant j \leqslant J
\tag{81}
$$

$$
[C_j] = \begin{bmatrix}
e_j & 0 & 0 & 0 & 0 & 0 & 0 \\
1 & 0 & 0 & 0 & 0 & 0 & 0 \\
0 & 1 & 0 & 0 & 0 & 0 & 0 \\
0 & 0 & 1 & 0 & 0 & 0 & 0 \\
(a_5)_j & (a_7)_j & (a_9)_j & 0 & 0 & 0 & 0 \\
(b_5)_j & (b_7)_j & 0 & 0 & 0 & 0 & 0 \\
(d_5)_j & 0 & (d_7)_j & 0 & 0 & 0 & 0
\end{bmatrix}, 1 \leqslant j \leqslant J-1
\tag{82}
$$

$$[\delta_1] = \begin{bmatrix} \delta v_0 \\ \delta s_0 \\ \delta q_0 \\ \delta f_0 \\ \delta v_0 \\ \delta s_0 \\ \delta q_0 \end{bmatrix}, [\delta_j] = \begin{bmatrix} \delta u_{j-1} \\ \delta g_{j-1} \\ \delta p_{j-1} \\ \delta f_j \\ \delta v_j \\ \delta s_j \\ \delta q_j \end{bmatrix}, [r_j] = \begin{bmatrix} (r_1)_{j-1/2} \\ (r_2)_{j-1/2} \\ (r_3)_{j-1/2} \\ (r_4)_{j-1/2} \\ (r_5)_{j-1/2} \\ (r_6)_{j-1/2} \\ (r_7)_{j-1/2} \end{bmatrix} 2 \leqslant j \leqslant J \quad (83)$$

The coefficient matrix A is known as a tridiagonal matrix due to the fact that all elements of $[A]$ are zero except those three along the diagonal. To solve Eq. (78), $[A]$ is assumed to be non-singular and can be factorized into

$$[A] = [L][U], \quad (84)$$

where

$$[L] = \begin{bmatrix} [I] & & & & \\ [\Gamma_2] & [I] & \ddots & & \\ & & \ddots & & \\ & & & \ddots & \\ & & & [I] & \\ & & & [\Gamma_j] & [I] \end{bmatrix}, \text{ and}$$

$$[U] = \begin{bmatrix} [\alpha_2] & [C_1] & & & \\ & [\alpha_2] & [C_2] & & \\ & & \ddots & \ddots & \\ & & & \ddots & \\ & & & [\alpha_{J-1}] & [C_{J-1}] \\ & & & & [\alpha_J] \end{bmatrix},$$

where $[I]$ is the identity matrix or order 7 and $[\alpha_i]$, $[\Gamma_i]$ are 7×7 matrices, whose elements are determined by the following relations:

$$[\alpha_1] = [A_1], \quad (85)$$

$$[A_1][\Gamma_1] = [C_1], \quad (86)$$

and

$$[\alpha_j] = [A_j] - [\Gamma_j][C_{j-1}], \quad j = 2, 3, \ldots J, \quad (87)$$

$$[\alpha_j][\Gamma_j] = [B_j]. \quad j = 2, 3, \ldots J, \quad (88)$$

Eq. (84) can be substituted into Eq. (78), which is

$$[L][U][\delta] = [r], \quad (89)$$

Now define

$$[U][\delta] = [W], \quad (90)$$

then Eq. (89) becomes

$$[L][W] = [r], \quad (91)$$

where

$$[W] = \begin{bmatrix} [W_1] \\ [W_2] \\ \vdots \\ [W_{J-1}] \\ [W_J] \end{bmatrix},$$

here $[W_j]$ are 7×1 column matrices. The element $[W]$ can be solved from Eq. (91)

$$[W_1] = [r_1], \quad (92)$$

$$[W_j] = [r_j] - [\Gamma_j][W_{j-1}], \quad 2 \leqslant j \leqslant J, \quad (93)$$

The step in which $[\Gamma_j]$, $[\alpha_j]$ and $[W_j]$ are calculated is usually referred to as a forward sweep. Once the elements of $[W]$ are found, Eq. (90) then gives the solution $[\delta]$ in the so-called backward sweep, in which the elements are obtained by the following relations:

$$[\delta_J] = [W_J], \quad (94)$$

$$[\delta_j] = [\alpha_j][W_j] - [C_j][\delta_{j+1}], \quad 2 \leqslant j \leqslant J, \quad (95)$$

These calculations are repeated until some convergence criterion is satisfied and iterations are stopped when

$$[\delta v_0^{(i)}] \leqslant \varepsilon_1, \quad (96)$$

where ε_1 is a small prescribed value. In this study, it is considered that $\varepsilon_1 = 0.00001$ which shows the accuracy of most predicted quantities up to four decimal places (Cebeci and Bradshaw, 1988).

Results and discussion

The set of nonlinear ordinary differential Eqs. (11)–(13) with boundary conditions (14) and (15) have been solved using Keller-box method. The effects of parameters of interest β, M, Gr_n, γ, Pr, R_d, N_b, N_t, Le and R on flow fields are analyzed. The accuracy of present method is assessed through comparison with the results of existing literature and displayed in Table 1.

Table 1 compares the values of skin friction coefficient for different values of m with those obtained by Yih [32], Cebeci and Bradshaw [30] and Mukhopadhyay and Mandal [27], observed in close agreement.

Figs. 3–6 are displayed to get insight of the physical behavior of β, M, Gr_n and γ on velocity profile, respectively. Fig. 3 exhibits that fluid velocity is higher for increasing values of β. However, the momentum boundary layer thickness is noticed as reduced. Physically, the plasticity of Casson fluid reduces when Casson parameter increases. Fig. 4 elucidates that momentum boundary layer thickness drops with the growth of M and K. The reason is that the resistance inside the fluid rises due to the increase in strength of Lorentz force and porosity of porous medium. Fig. 5 presents that fluid velocity accelerates with increment in Gr_n. Since thermal force assists the fluid velocity therefore leads to reduces thermal boundary layer thickness. On the other hand, Fig. 6 portrays that fluid velocity is higher when $\gamma > 0$ and reduces when $\gamma < 0$. It is also observed that the momentum boundary layer shorten in $\gamma > 0$ case.

Figs. 7–10 illustrate the variation of Pr, R_d, N_b and N_t on temperature profile, respectively. Fig. 7 depicts that increasing values of Pr reduces the thermal diffusion and enhances the thermal capacity of fluid, accordingly dimensionless temperature dropped. Clearly, Fig. 8 shows that the fluid temperature is an increasing function of R_d in both cases of $M = 0$ and $M = 1$. It is well known that increase in radiation parameter enhance the energy transport inside the fluid. Consequently, rate of heat transfer at the surface increased. From Figs. 9 and 10 determine a slight increase in dimensionless temperature for increasing values of N_b and N_t. It is well known that strength of N_b raises the thermal conductivity of base fluid and strength of N_t generates the thermophoretic force due to temperature gradient, which causes a rapid flow away from the wedge. Therefore, hot fluid is moved away from the wedge surface, and so thermal boundary layer becomes thicker.

To get insight the effect of N_b, N_t, Le and R on nanoparticles concentration profile, Figs. 11–14 are depicted, respectively. Figs. 11 and 12 reveal that strength of N_b declines the concentration boundary layer thickness, whereas concentration boundary layer becomes thicker with increase in N_t. Physically, it is justified

Table 1
Comparison of skin friction coefficient $f''(0)$ for various values of m for Newtonian Fluid with $M = K = Gr_n = Gm_n = R_d = \delta = \gamma = 0$.

$f''(0)$				
m	Yih [32]	Cebeci and Bradshaw [30]	Mukhopadhyay and Mandal [27]	Present results
−0.05	0.213484	0.21351	0.213802	0.21321
0.0	0.332057	0.33206	0.332206	0.33206
0.3333	0.757448	0.75745	0.757586	0.75743
1	1.232588	1.23259	1.232710	1.23259
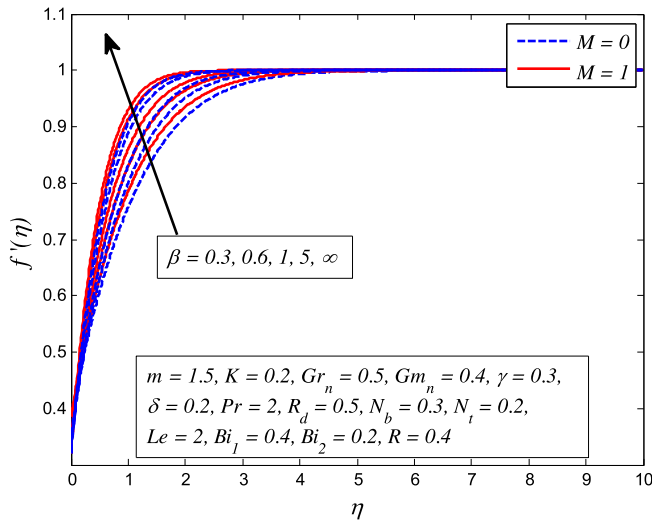
Fig. 3. Variation of β on velocity profile for different values of M.
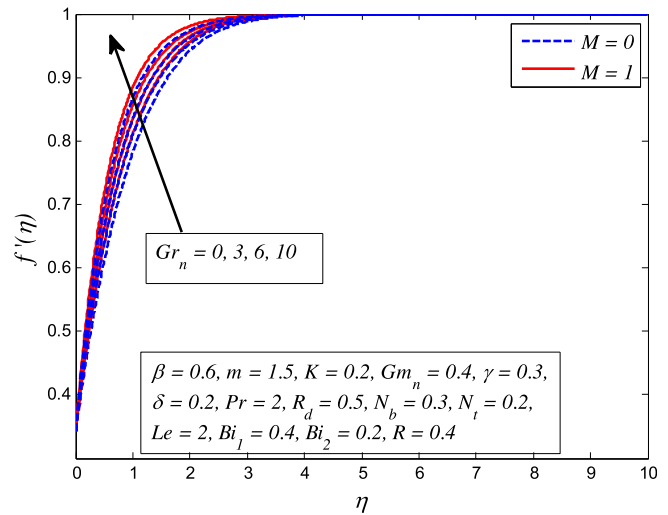
Fig. 5. Variation of Gr_n on velocity profile for different values of M.
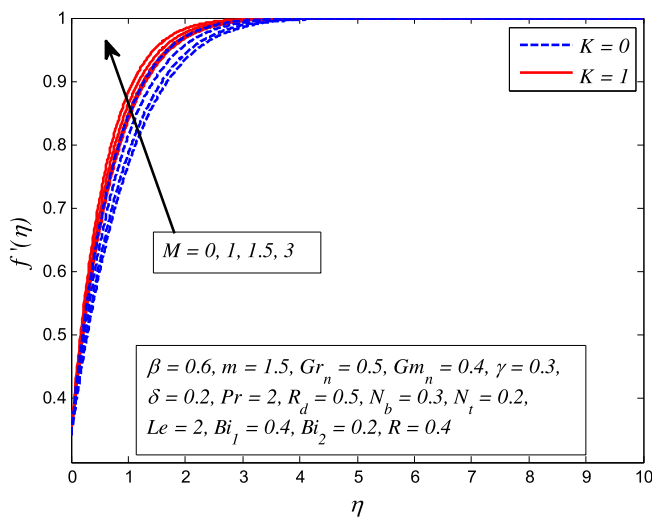
Fig. 4. Variation of M on velocity profile for different values of K.
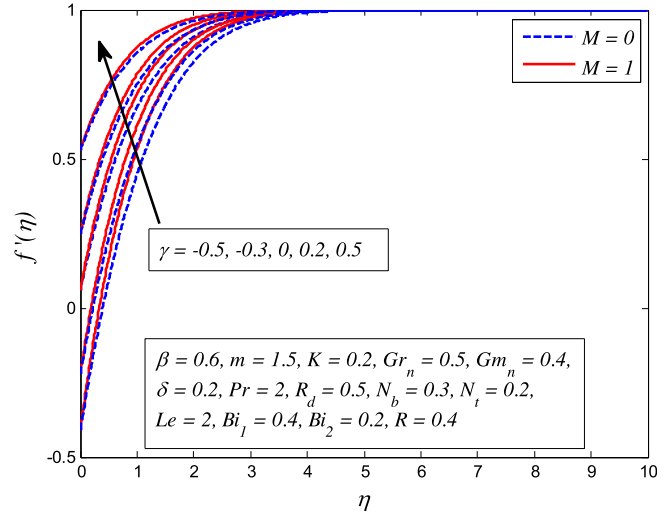
Fig. 6. Variation of γ on velocity profile for different values of M.

because Brownian motion occurs due to the interaction of nanoparticles with base fluid in a nanofluid system. The reason is that the Brownian diffusion exhibits heat conduction. The nanoparticles enhance the wedge surface area for heat transfer. A nanofluid is a two-phase system where the random motion of nanoparticles enhances the kinetic energy. Nevertheless, nanoparticles diffusion strongly influenced with the Brownian motion. On the other hand, thermophoresis phenomenon leads to disperse the nanoparticles from the hot surface to the ambient fluid, since the nanometer size particles experience resistance from heated surface. Therefore, the thermophoretic force permits nanoparticles to import heat from the surface to the moving fluids. Consequently,

thicken concentration boundary layer. Fig. 13 examines that nanoparticles concentration is a decreasing function of Le. Since stronger Lewis number intimates a weaker Brownian diffusion coefficient which result relatively small penetration depth for the concentration boundary layer. On the contrary, Fig. 14 presents that nanoparticles concentration rises when $R < 0$, whereas opposite is seen when $R > 0$. The destructive chemical reaction within the boundary layer has the tendency to decrease the nanoparticles concentration.

Figs. 15–18 are plotted to analyze the variation of skin friction coefficient, Nusselt number and Sherwood number for different values of β, M, K, Gr_n, γ, Pr, R_d, Le and R, respectively. Fig. 15
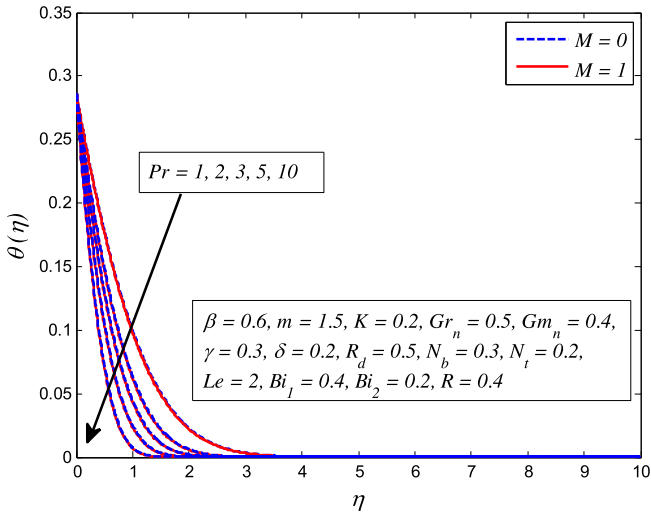
Fig. 7. Variation of Pr on temperature profile for different values of *M*.
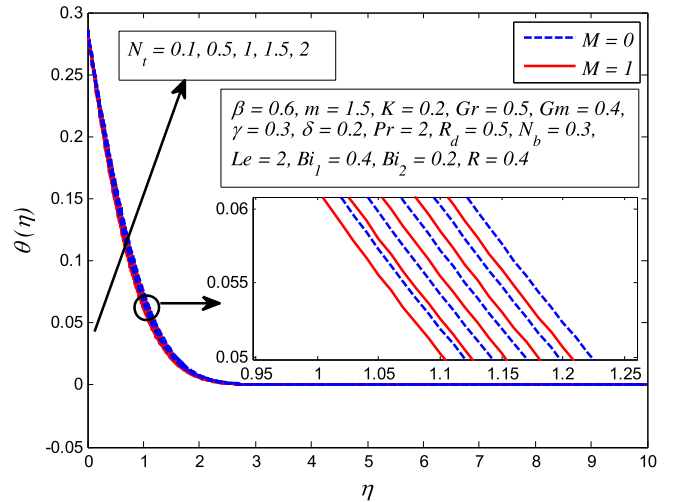

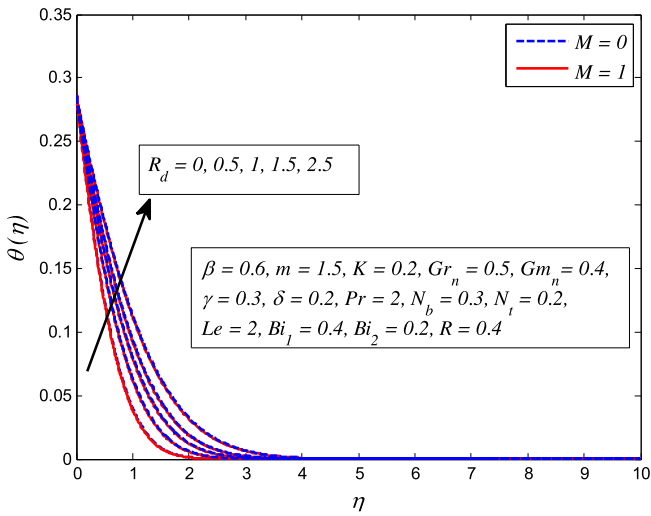**Fig. 10.** Variation of N_t on temperature profile for different values of *M*.

Fig. 8. Variation of R_d on temperature profile for different values of *M*.
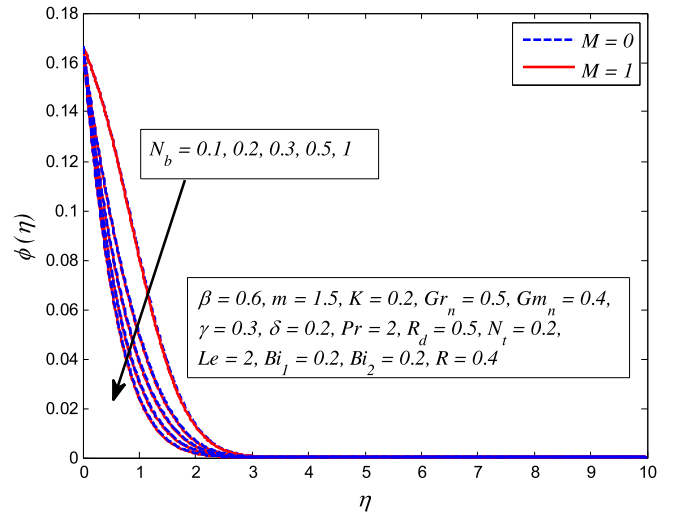

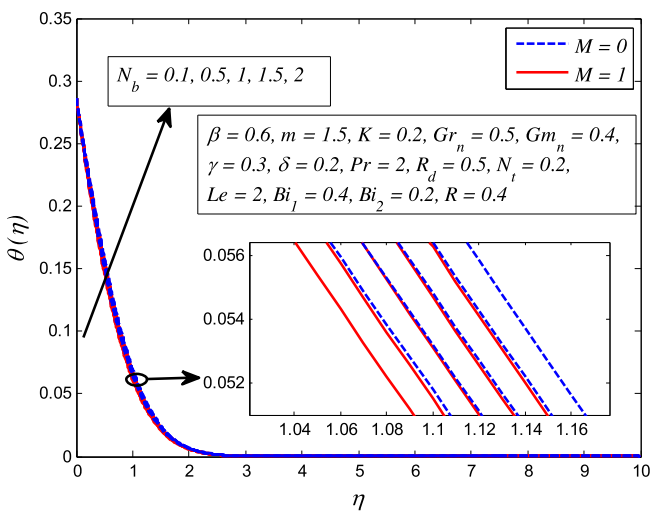**Fig. 11.** Variation of N_b on nanoparticles concentration for different values of *M*.

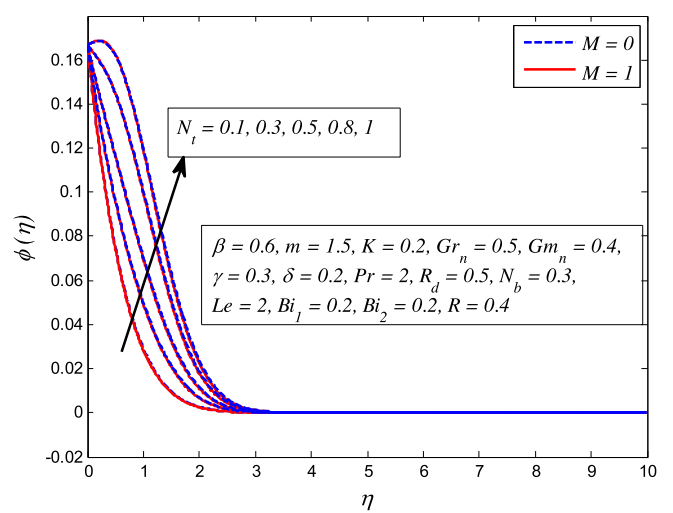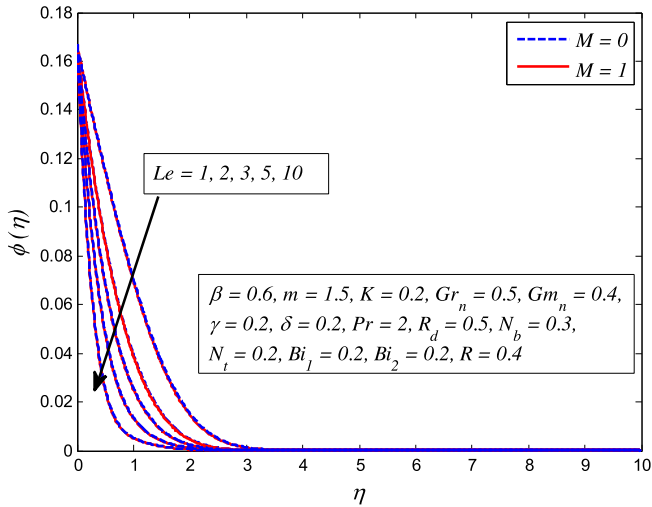**Fig. 9.** Variation of N_b on temperature profile for different values of *M*.

Fig. 12. Variation of N_t on nanoparticles concentration for different values of *M*.

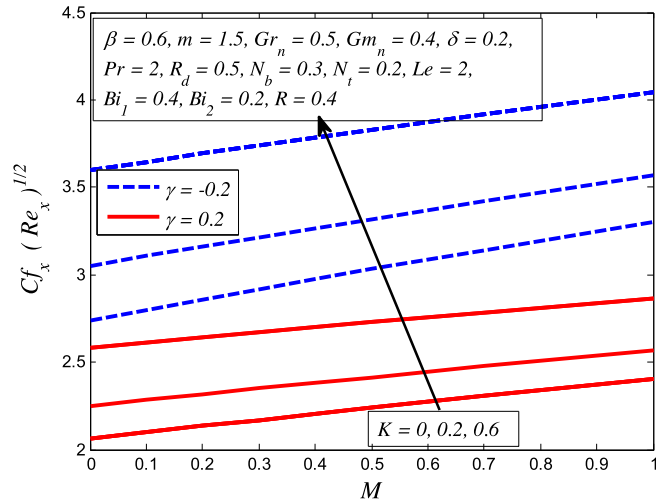**Fig. 13.** Variation of *Le* on nanoparticles concentration for different values of *M*.

Fig. 14. Variation of *R* on nanoparticles concentration for different values of *M*.

Fig. 15. Variation of skin friction coefficient for different values of *β*, *M* and *Gr*.
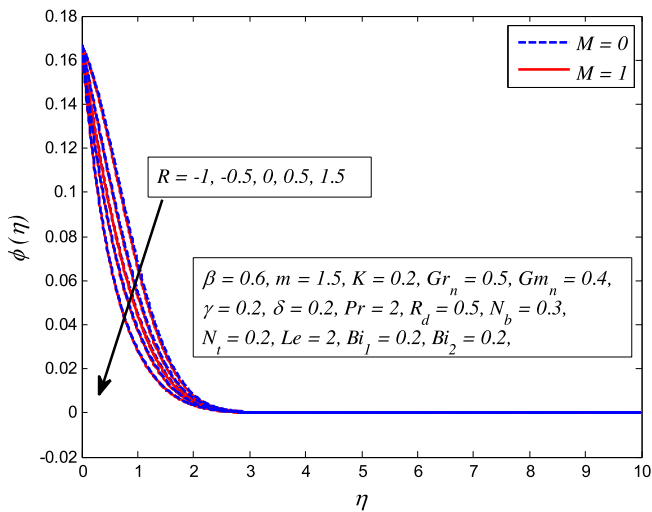

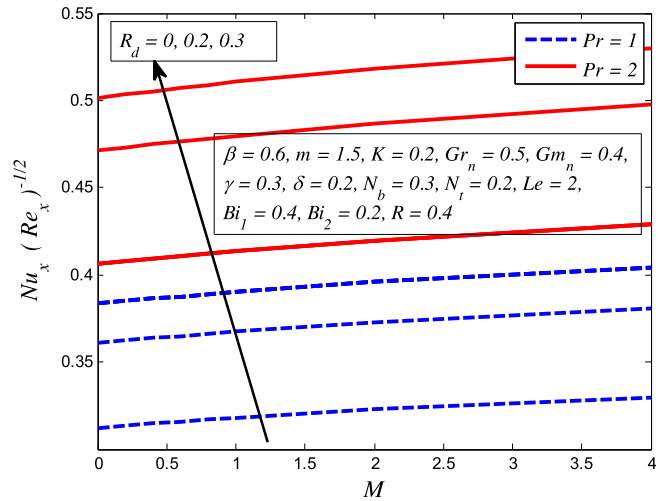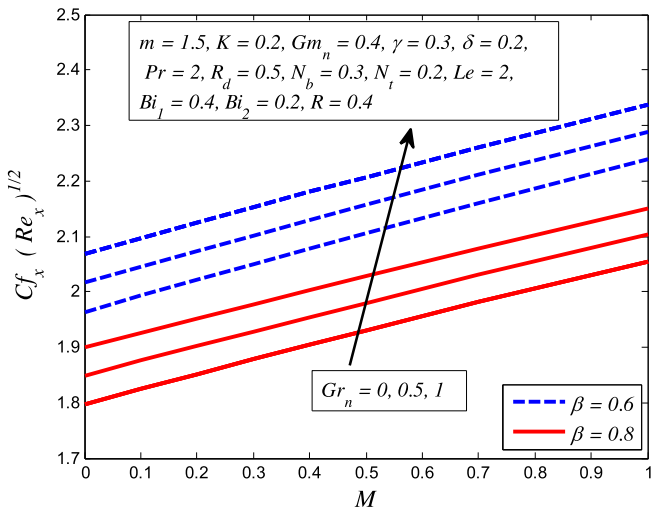**Fig. 16.** Variation of skin friction coefficient for different values of *K*, *γ* and *M*.

Fig. 17. Variation of Nusselt number for different values of Pr, MR_d and *M*.
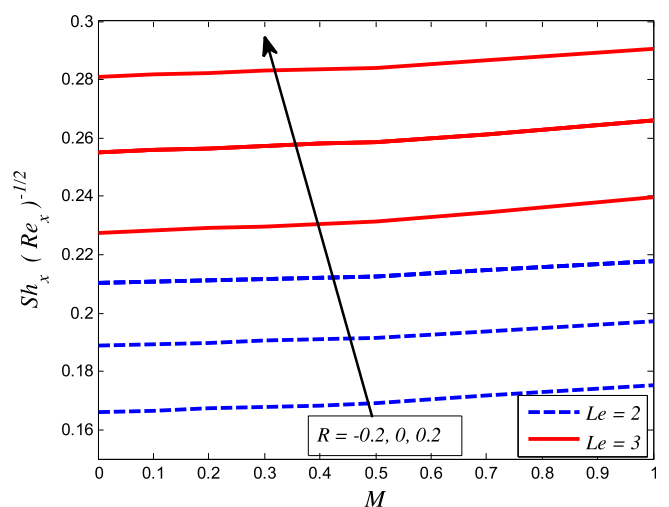

Fig. 18. Variation of Sherwood number for different values of *Le*, *R* and *M*.

presents that the wall shear stress is higher for higher values of β and M, while reverse trend is noticed for β. On the other hand, it is evident from Fig. 16 that friction factor falls when $\gamma > 0$ and rises when $\gamma < 0$. This figure also clears that the strength of K caused a progressive enhancement in friction factor. From Fig. 17, it is noted that higher values of Pr and R_d boost the heat transfer rate, whereas this increase is noticed less with the variation of M. Fig. 18 demonstrates that increasing values of Sc and R assists the mass transfer rate.

Conclusions

In present work, the two dimensional electrically conducting mixed convection flow of Casson fluid over a wedge saturated in nanoparticles is investigated. The effect of thermal radiation in the presence of slip and convective boundary conditions is also analyzed. The nonlinear governing equations are transformed through suitable transformations and the numerical computations are carried out via Keller box method. The algorithm is developed in MATLAB software and validated through comparison with the results in existing literature. A very close agreement is observed. The effect of physical parameters, namely, Casson parameter β, magnetic parameter M, thermal Grashof number Gr_n, Prandtl number Pr, radiation parameter R_d, Brownian motion parameter N_b, thermophoresis parameter N_t, Lewis number Le, chemical reaction parameter R and moving wedge parameter γ are discussed and displayed graphically. Some of the interesting findings from this research are as follow:

1. Increase in β and M thinning the momentum boundary layer thickness.
2. Increase in N_b and N_t slightly enhanced the thermal boundary layer thickness.
3. The variation of M on heat and mass transfer rates is not profoundly as wall shear stress.
4. The effect of N_b and N_t on nanoparticles concentration is observed opposite.
5. The wall shear stress is observed to be enhanced with increase in M and K.
6. The influence of Pr and Le on heat and mass transfer rates is noticeable.

Acknowledgement

Conflict of interest

The authors of this manuscript have no conflict of interest.

References

[1] Choi SUS, Eastman JA. Enhancing thermal conductivity of fluids with nanoparticles. Proc 1995 ASME Int Mech Engineering Congr Expo SanFrancisco, USA, ASME, FED231/MD66. 1995:99-105.

[2] Buongiorno J. Convective transport in nanofluids. ASME J Heat Transf 2006;128(3):240–50. https://doi.org/10.1115/1.2150834.

[3] Nield D, Kuznetsov A. The Cheng-Minkowycz problem for natural convective boundary-layer flow in a porous medium saturated by a nanofluid. Int J Heat Mass Transf 2009;52(25–26):5792–5. https://doi.org/10.1016/j.ijheatmasstransfer.2009.07.024.

[4] Yacob NA, Ishak A, Nazar R, Pop I. Falkner-Skan problem for a static and moving wedge with prescribed surface heat flux in a nanofluid. Int Commun Heat Mass Transf 2011;38(2):149–53. https://doi.org/10.1016/j.icheatmasstransfer.2010.12.003.

[5] Khan WA, Hamad MAA, Ferdows M. Heat transfer analysis for Falkner-Skan boundary layer nanofluid flow past a wedge with convective boundary condition considering temperature-dependent viscosity. J Nanoeng Nanosyst 2012;227(1):19–27. https://doi.org/10.1177/1740349912459131.

[6] Chamkha AJ, Abbasbandy S, Rashad AM, Vajravelu K. Radiation effects on mixed convection about a cone embedded in a porous medium filled with a nanofluid. Meccanica 2013;48(2):275–85. https://doi.org/10.1007/s11012-012-9599-1.

[7] RamReddy C, Murthy PVSN, Chamkha AJ, Rashad AM. Soret effect on mixed convection flow in a nanofluid under convective boundary condition. Int J Heat Mass Transf 2013;64:384–92. https://doi.org/10.1016/j.ijheatmasstransfer.2013.04.032.

[8] Kasmani RM, Sivasankaran S, Bhuvaneswari M, Siri Z. Effect of chemical reaction on convective heat transfer of boundary layer flow in nanofluid over a wedge with heat generation/absorption and suction. J Appl Fluid Mech 2016;9(1):379–88.

[9] Sandeep N, Animasaun IL. Heat transfer in wall jet flow of magnetic-nanofluids with variable magnetic field. Alexandria Eng J 2017;56:263–9. https://doi.org/10.1016/j.aej.2016.12.019.

[10] Chamkha AJ. Non-darcy hydromagnetic free convection from a cone and a wedge in porous media. Int Commun Heat Mass Transf 1996;23(6):875–87.

[11] Takhar HS, Chamkha A, Nath G. Unsteady flow and heat transfer on a semi-infinite flat plate with an aligned magnetic field. Int J Eng Sci 1999;37:1723–36.

[12] Takhar HS, Chamkha AJ, Nath G. MHD flow over a moving plate in a rotating fluid with magnetic field, hall currents and free stream velocity. Int J Eng Sci 2002;40(13):1511–27. https://doi.org/10.1016/S0020-7225(02)00016-2.

[13] Al-Mudhaf A, Chamkha AJ. Similarity solutions for MHD thermosolutal Marangoni convection over a flat surface in the presence of heat generation or absorption effects. Heat Mass Transfer 2005;42(2):112–21. https://doi.org/10.1007/s00231-004-0611-8.

[14] Chamkha AJ, Mujtaba M, Quadri A, Issa C. Thermal radiation effects on MHD forced convection flow adjacent to a non-isothermal wedge in the presence of a heat source or sink. Heat Mass Transfer 2003;39:305–12. https://doi.org/10.1007/s00231-002-0353-4.

[15] Nandy SK, Mahapatra TR. Effects of slip and heat generation/absorption on MHD stagnation flow of nanofluid past a stretching/shrinking surface with convective boundary conditions. Int J Heat Mass Transfer 2013;64:1091–100. https://doi.org/10.1016/j.ijheatmasstransfer.2013.05.040.

[16] Rashidi MM, Vishnu Ganesh N, Abdul Hakeem AK, Ganga B. Buoyancy effect on MHD flow of nanofluid over a stretching sheet in the presence of thermal radiation. J Mol Liq 2014;198:234–8. https://doi.org/10.1016/j.molliq.2014.06.037.

[17] Chamkha AJ, Rashad AM. MHD forced convection flow of a nanofluid adjacent to a non-isothermal wedge. Comput Therm Sci 2014;6(1):27–39. https://doi.org/10.1016/S0735-1933(99)00070-6.

[18] Chamkha AJ, Rashad AM. Natural convection from a vertical permeable cone in a nanofluid saturated porous media for uniform heat and nanoparticles volume fraction fluxes. Int J Numer Methods Heat Fluid Flow 2012;22(8):1073–85. https://doi.org/10.1108/09615531211271871.

[19] Chamkha AJ. Coupled heat and mass transfer by natural convection ab out a truncated cone in the presence of m agnetic field and radiation effects. Numer Heat Transf 2001;39:511–30.

[20] Takhar HS, Chamkha AJ, Nath G. Unsteady mixed convection flow from a rotating vertical cone with a magnetic field. Heat Mass Transf 2003;39(4):297–304. https://doi.org/10.1007/s00231-002-0400-1.

[21] Chamkha AJ, Al-Mudhaf A. Unsteady heat and mass transfer from a rotating vertical cone with a magnetic field and heat generation or absorption effects. Int J Therm Sci 2005;44(3):267–76. https://doi.org/10.1016/j.ijthermalsci.2004.06.005.

[22] Chamkha AJ, Abbasbandy S, Rashad AM, Vajravelu K. Radiation effects on mixed convection over a wedge embedded in a porous medium filled with a nanofluid. Transp Porous Media 2012;91(1):261–79. https://doi.org/10.1007/s11242-011-9843-5.

[23] Khan M, Karim I, Islam M, Wahiduzzaman M. MHD boundary layer radiative, heat generating and chemical reacting flow past a wedge moving in a nanofluid. Nano Converg 2014;1(1):20. https://doi.org/10.1186/s40580-014-0020-8.

[24] Pandey AK, Kumar M. Effect of viscous dissipation and suction/injection on MHD nanofluid flow over a wedge with porous medium and slip. Alexandria Eng J 2016;55(4):3115–23. https://doi.org/10.1016/j.aej.2016.08.018.

[25] Damseh RA, Al-Odat MQ, Chamkha AJ, Shannak BA. Combined effect of heat generation or absorption and first-order chemical reaction on micropolar fluid flows over a uniformly stretched permeable surface. Int J Therm Sci 2009;48(8):1658–63. https://doi.org/10.1016/j.ijthermalsci.2008.12.018.

[26] Chamkha AJ, Mohamed RA, Ahmed SE. Unsteady MHD natural convection from a heated vertical porous plate in a micropolar fluid with Joule heating, chemical reaction and radiation effects. Meccanica 2011;46(2):399–411. https://doi.org/10.1007/s11012-010-9321-0.

[27] Mukhopadhyay S, Mandal IC. Boundary layer flow and heat transfer of a Casson fluid past a symmetric porous wedge with surface heat flux. Chin Phys B 2014;23(4):44702. https://doi.org/10.1088/1674-1056/23/4/044702.

[28] Ibrahim SM, Lorenzini G, Kumar VP, Raju CSK. Influence of chemical reaction and heat source on dissipative MHD mixed convection flow of a Casson nanofluid over a nonlinear permeable stretching sheet. Int J Heat Mass Transf 2017;111(4):346–55. https://doi.org/10.1016/j. ijheatmasstransfer.2017.03.097.

[29] Raju CSK, Sandeep N. Nonlinear radiative magnetohydrodynamic Falkner-Skan flow of Casson fluid over a wedge. Alexandria Eng J 2016;55(3):2045–54. https://doi.org/10.1016/j.aej.2016.07.006.

[30] Cebeci T, Bradshaw P. Physical and computational aspects of convective heat transfer. 1st ed. New York: Springer, New York; 1988.

[31] Roşca NC, Roşca AV, Pop I. Stagnation point flow and heat transfer over a non-linearly moving flat plate in a parallel free stream with slip. Commun Nonlinear Sci Numer Simul 2014;19(6):1822–35. https://doi.org/10.1016/j. cnsns.2013.10.019.

[32] Yih KA. MHD forced convection flow adjacent to a non-isothermal wedge. Int Commun Heat Mass Transf 1999;26(6):819–27. https://doi.org/10.1016/ S0735-1933(99)00070-6.